J Mater Sci (2009) 44:5609–5617
DOI 10.1007/s10853-009-3790-3

Reaction progress of alkaline-activated metakaolin-ground granulated blast furnace slag blends

Anja Buchwald · R. Tatarin · D. Stephan

Received: 20 February 2009 / Accepted: 1 August 2009 / Published online: 13 August 2009

Abstract Ground granulated blast furnace slag (ggbf slag) and metakaolin were blended and the combination was activated by sodium hydroxide solution. Two mix series were investigated, one with low NaOH concentration (9–16 wt%) and the other with a high NaOH concentration of 25 wt%. The reaction progress of the alkali-activated pastes was indirectly measured by isothermal calorimetry as well as by ultrasonic measurements. Both methods show an acceleration of the condensation reaction of the alkali-activated blends compared to both single phases. The acceleration effect is more considerable at the higher activator concentration related to a higher reaction degree of the metakaolin.

Introduction

The alkaline activation of reactive alumosilicate materials yields to a hardening process and the formation of a cement stone that can be used for the production of concrete. Several raw materials are suitable in this way for instance metakaolin [1, 2], fly ashes and slags; but mainly fly ashes and ground granulated blast furnace slags (ggbf slags) [3, 4] are used commercially as building materials. The reaction products of alkali-activated materials are different depending on the calcium content of the activated material. The alkaline activation of calcium-free materials such as metakaolin and some fly ashes results in the formation of amorphous to semi-crystalline three-dimensional alumosilicate networks by polycondensation [2]. These binders are also known as "geopolymers" as named by Davidovits [1]. The reaction product of ggbf slag have been widely investigated and can be compared to calcium silicate hydrates (C–S–H) from Portland cements, apart from incorporated tetrahedral aluminium into the dreierketten structure of the calcium silicate hydrates [5–7] and hydrotalcite if the slag contains magnesium [8].

The possibility of a simultaneous formation of C–S–H and aluminosilicate phases in metakaolin/lime mixtures has been shown to depend on the alkalinity of the system [9, 10]. Yip and van Deventer [11, 12] found in their investigation on metakaolin/slag blends that C–S–H phases and aluminosilicate gel coexist. Structural investigations of the reaction products formed by the alkaline activation of metakaolin—ggbf slag blends [13] showed that there is not only the coexistence of alumosilicate network (ASN) and C–S–H, but also an additional incorporation of aluminium tetrahedra into the C–S–H. That results in a longer chain length of the (alumina-) silicate chains.

Within the investigation presented here, the reaction progress was indirectly measured by isothermal calorimetry as well as by ultrasonic measurements.

A. Buchwald
Building Chemistry, Bauhaus-University Weimar,
Coudraystr. 13C, 99421 Weimar, Germany

Present Address:
A. Buchwald (✉)
ASCEM B.V., Holleweg 19, 6191 RA Beek, The Netherlands
e-mail: a.buchwald@ascem.nl

R. Tatarin
F.A. Finger-Institute for Building Materials Science,
Bauhaus-University Weimar, Weimar, Germany

D. Stephan
Group of Building Materials and Building Chemistry,
Technical University Kassel, Kassel, Germany

Experimental

Material characteristics, composition and preparation

Ggbf slag (S) and commercially available metakaolin Metastar 402 from Imerys GB (M) were used as raw materials. The chemical composition and physical properties are given in Tables 1 and 2. In order to determine the phase composition by X-ray diffraction, the metakaolin or the ggbf slag was mixed with a standard material (about 10% ZnO by weight) and ground under the addition of isopropanol in a bar mill (McCrone-Micronizer, McCrone Ltd., UK) for about 1 min. This mill was used to avoid preferred orientation (texture) and the introduction of stress. CuKα radiation was used to measure X-ray diffraction. Quantification was carried out using Rietveld refinement (Autoquant®). As can seen in Fig. 1, the ggbf slag consists of 73 wt% glass as well as crystalline calcium silicate phases and a considerable amount of calcite. Besides the crystalline phases feldspar, quartz and muscovite, 84 wt% of the metakaolin is amorphous attributed to dehydroxylated kaolinite.

Metakaolin and ggbf slag as well as their blends were activated with sodium hydroxide solution as summarised in Table 3. The 25M/75S blend consists of 25 wt% metakaolin and 75 wt% ggbf slag, the 50M/50S blend consists of 50 wt% metakaolin and 50 wt% ggbf slag. Two mix series were investigated:

Table 1 Chemical composition of the raw materials

	ggbf slag (wt%)	Metakaolin (wt%)
L.o.I. (1,000 °C)	4.91	1.0
SiO_2	31.34	52.1
Al_2O_3	10.39	43.0
Fe_2O_3	1.08	0.7
CaO	42.61	0.0
MgO	7.52	0.3
K_2O	0.66	2.5
Na_2O	0.25	0.12
Cl	0.03	n.d.
SO_3	1.08	n.d.
P_2O_5	0.13	n.d.

n.d. not determined

Table 2 Physical properties of the raw materials

	Density (g/cm^3)	Surface area, measured by		Mean grain size (μm)
		Blaine (cm^2/g)	BET (cm^2/g)	
ggbf slag (S)	2.9	8,120		15.8
Metakaolin (M)	2.55		11,600	3.9

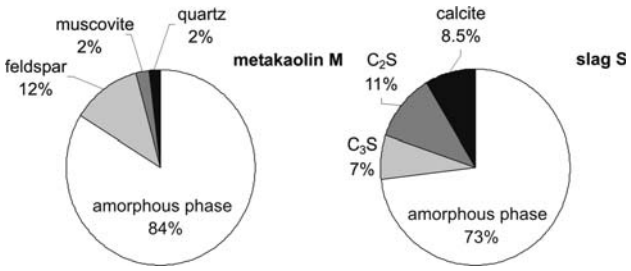

Fig. 1 Mineral composition of the metakaolin and the ggbf slag

- *Series A:* It is used low concentrated alkaline solutions between 9.2 and 15.7 wt% NaOH. The concentration was calculated to reach the same Na/Al value of 0.4 according to the chemical composition of the metakaolin, the ggbf slag and their blends. The water content was adjusted to give the same workability of the pastes; therefore, the water content varies. The workability was measured by using a flow table.
- *Series B*: The concentration of the NaOH solution was increased to 25.4 wt% (8 mol/L) and kept constant for all blends in order to reach a higher reaction degree as in series A [13, 14]. The same solution volume is used as in series A.

The detailed mixtures are given in Table 3. The water/binder-ratio ($w/b = m_{water}/m_{(S+M)}$) ranges from 0.32 for the pure slag-B mix to 0.77 for the pure metakaolin B-mix due to the different density of the solid raw materials and the activator as well (see Table 3). The corresponding % Na_2O characteristics of the mixes are noticed for comparison. The same composition was used within both the calorimetric and the ultrasonic measurements, except for mixtures B that were slightly changed for the ultrasonic measurements by increasing the activator volume to achieve a good homogeneity. The adjusted solution volume is given in Table 3 in brackets.

Mixing took place externally by manual mixing until a good homogeneity was achieved.

All measurements were carried out under isothermal conditions at 20 °C. For ultrasonic measurements, the covering of the specimens and storage in a climatic chamber at 95% RH were applied to prevent drying.

Calorimetric measurements

Calorimetric measurements are used to follow the progress of reaction in terms of heat evolution. It is a standard method in cement science and was occasionally used for the characterisation of alkali-activated binders [15–18].

An isothermal heat-conduction calorimeter (TAM air, Thermometric, Järfälla, Sweden) was used to measure the heat of reaction. The heat evolution of pastes was

Table 3 Composition of alkali-activated blends

	Mix composition			Characteristics			
	Metakaolin (g)	Slag (g)	NaOH sol. (mL)	NaOH solution		Paste	
				NaOH-content (wt%)	Density (g/mL)	*w/b* ratio (g/g)	% Na_2O[a] (%)
A-S		6	2	9.2	1.10	0.33	2.6
A-M25/S75	1.5	4.5	2.6	12	1.13	0.43	4.6
A-M50/S50	3	3	3.1	13.7	1.15	0.51	6.3
A-M	6		4.3	15.7	1.17	0.71	10.2
B-S		6	2 (2.4)[b]	25.4	1.27	0.32 (0.37)[b]	8.4 (9.8)[b]
B-M25/S75	1.5	4.5	2.6 (2.9)[b]	25.4	1.27	0.41 (0.47)[b]	10.9 (12.3)[b]
B-M50/S50	3	3	3.1 (3.5)[b]	25.4	1.27	0.49 (0.56)[b]	13.0 (14.8)[b]
B-M	6		4.3 (4.7)[b]	25.4	1.27	0.68 (0.77)[b]	18.0 (19.7)[b]

[a] % Na_2O—mass Na_2O per mass (slag + metakaolin) * 100%

[b] In brackets: differing composition for ultrasonic measurements

investigated at 20 ± 0.1 °C over 74 h. The pastes were mixed externally. The paste compositions are given in Table 3.

Ultrasonic measurements

The acoustic method of ultrasonic through transmission was used in the investigations. This method is well established for investigation of stiffening and hardening of cementitious materials such as cement paste, mortar and concrete [19, 20] but so far not applied to geopolymers. Lawson [21, 22] recently applied ultrasonic techniques to evaluate elastic properties of alkali-activated metakaolin with variable Si/Al-ratio. Measurements of longitudinal and shear wave velocities were carried out to determine the elastic modulus and Poisson's ratio on hardened samples. Lawson [21] recommended ultrasonic measurements of the fresh pastes during setting.

Generally mechanical waves in the ultrasonic range are generated by a sound source and transmitted to the test piece. A sound field is produced corresponding to the nature of the excitation. It is propagated and influenced in a way that is characteristic for the current microstructure of the sample. After through transmission, the sound field parameters are measured at the sound receiver. The structure forming processes that are macroscopically indicated by the setting and hardening cause a considerable change of the acoustic transmission behaviour of the sample. In order to describe material properties, the ultrasonic parameters longitudinal wave velocity and amplitude as well as the transmitted frequency content can be used [19]. The wave velocities are functions of the elastic properties of the specimen. In hardened state, the p-wave velocity is related to the dynamic Young's modulus E, the density ρ of the material and the Poisson's ratio v according to Eq. 1:

$$v_p = \sqrt{\frac{E \cdot (1-v)}{p \cdot (1-2v) \cdot (1+v)}}. \quad (1)$$

Young's modulus and Poisson's ratio change significantly during the solidification of the binder. An independent determination of both, the Young's modulus and Poisson's ratio, can only be determined by application of a second elastic wave (e.g. shear waves). Nonetheless, the solidification can be continuously followed without the knowledge of Poisson's ratio solely by means of p-wave velocities curves. In this case, differences in the mixture composition in terms of water/binder-ratio and solid density between samples can confine the comparability of absolute values of the p-wave velocity. For example, two identical performing specimens with equal Young's Modulus and Poisson's ratio will show different longitudinal wave velocities if different densities due to a different water/cement ratio are used.

The measurement set-up used in this investigation is illustrated in Fig. 2. The testing container employed was especially designed for investigation of minor specimen quantities as used for the hydration reaction of synthetic cement clinker minerals. It consists of two parallel side walls with affixed piezoelectric transducers. Between the side walls, a closed-cell EPDM foam is clamped to keep fresh specimen in a block-shaped receptacle.

The excitation of elastic waves by the transmitter is based on the inverse piezoelectric effect and can be characterised as multi-resonant with broad frequency content up to 500 kHz. For excitation, a high voltage pulse is used at the ultrasonic generator. Excitation time is one-fourth of a 350 kHz sine period. The signals are then captured by means of an external 12 bit/40 MHz A/D-converter and stored for further parameter analysis. Averaging in time domain was applied to improve signal to noise ratio by a

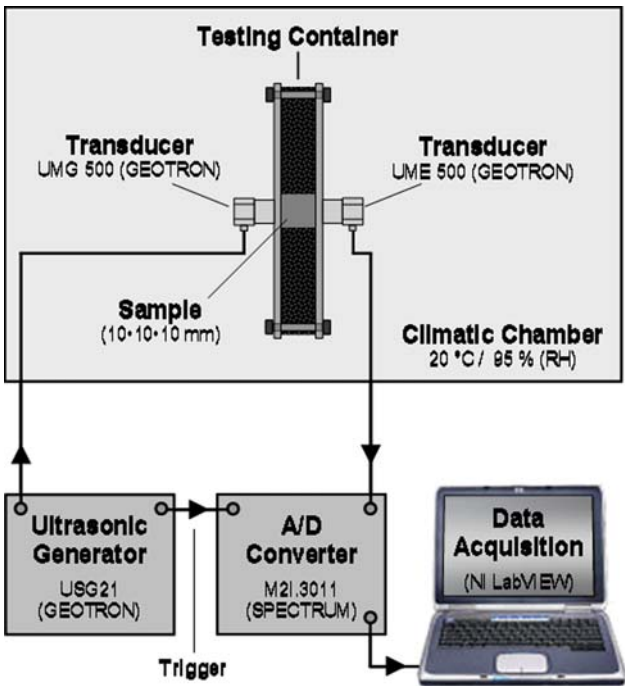

Fig. 2 Experimental set-up and testing container for ultrasonic through transmission following the early hydration of paste samples

factor of $n^{0.5}$; n is the numbers of single measurements. The onset of the p-wave was evaluated from the measured data and p-wave velocities were determined from the pulse transit times.

By modelling the measured p-wave curves mathematically, smoothed curve progressions can be achieved and the comparison of different samples becomes more practicable. In addition characteristic points (e.g. by first and second derivative) can be determined accurately [20]. Logistic functions can be used to represent s-shaped wave velocities curves as proposed by Grosse et al. [20]. Such functions describe curves that initially rise exponentially until the increase becomes gradually decelerated by feedback mechanisms. Equation 2 superposes three logistic functions with different gradients, points of inflections, initial and end values, respectively,

$$v(t) = \frac{k_1}{1 + e^{(t-t_1)/\mathrm{d}t_1}} + \frac{k_2}{1 + e^{(t-t_2)/\mathrm{d}t_2}} + \frac{k_3}{1 + e^{(t-t_3)/\mathrm{d}t_3}} + c. \tag{2}$$

The parameter k_n $(n = 1\ldots3)$ of the multi-logistic function is the difference of p-wave velocities at $t = -\infty$ and $t = \infty$ of the single logistic function. The time t_n $(n = 1\ldots3)$ is associated with the centre point between these p-wave velocities and $\mathrm{d}t_n$ $(n = 1\ldots3)$ is the gradient at t_n. This function results in a parameter set of 10 values for each sample including a constant c, which were determined iteratively by using the method of least squares.

Results

Calorimetric measurements

As shown in literature, the heat evolution vs. time diagram has a different shape depending on the used activator as discussed by Shi [24]. Figures 3 and 4 illustrate the measured heat flow/per mass data (Figs. 3a, 4a) as well as the cumulated heat (Figs. 3b, 4b) of the mix series A and B. Therein, the expected curve shape of the heat evolution of NaOH-activated slag [17, 18] and metakaolin [15, 16, 23] systems are recognisable. The curve consists of two peaks, one initial sharp peak that passes over into a broader second peak. There is no induction period between both peaks detectable. The first peak can be addressed to the wetting of the solid surface together with the dissolution, whereas the second peak shows the heat evolution of the condensation process [23, 24], either to the calcium silicate hydrates (C–S–H) or to the alumosilicate network (ASN).

Generally, the heat flow achieved higher values for series B; therein, the higher concentrated activator was used.

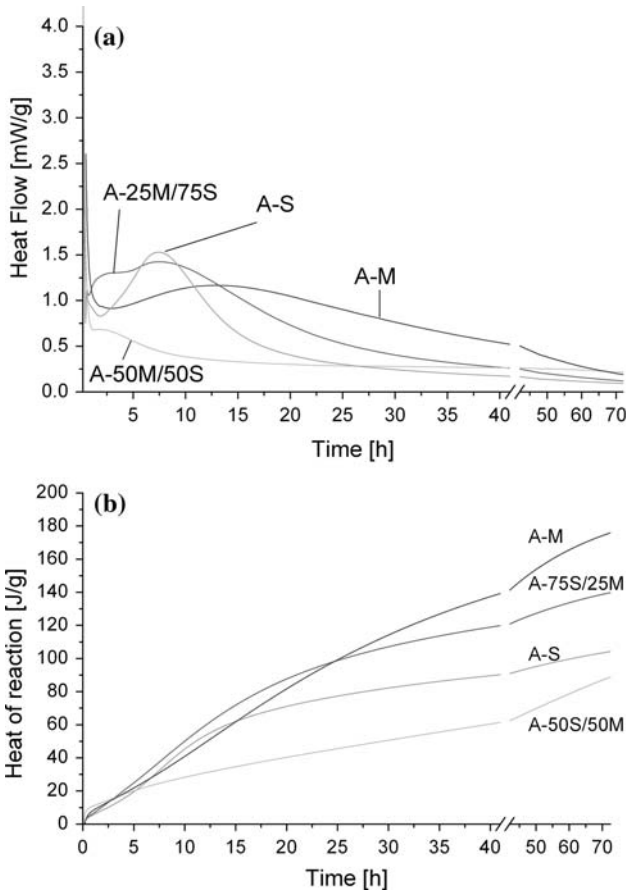

Fig. 3 Results of calorimetric measurements at low NaOH concentration—series A. **a** Heat flow, **b** cumulated heat versus time

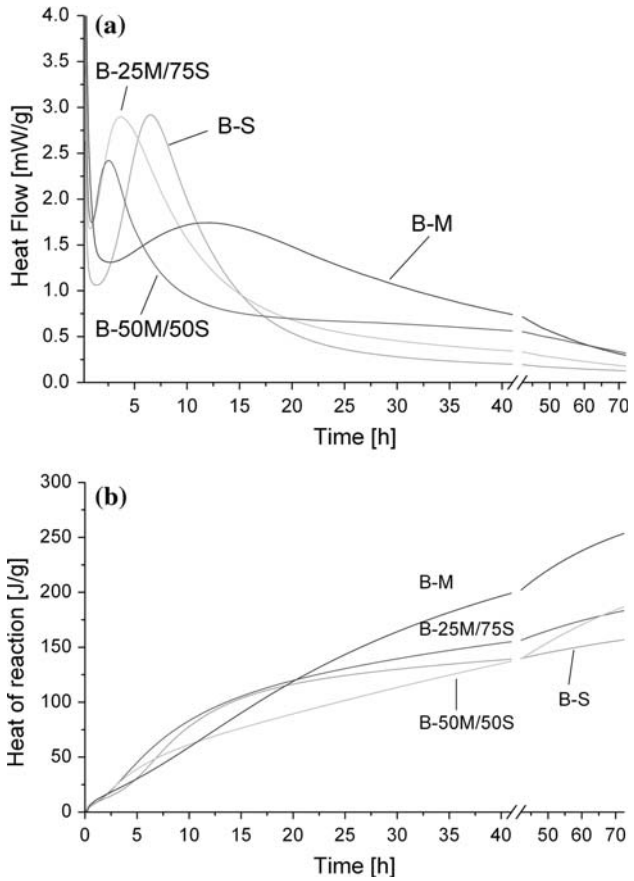

Fig. 4 Results of calorimetric measurements at high NaOH concentration—series B. **a** Heat flow, **b** cumulated heat versus time

The pure metakaolin pastes (A-M and B-M) are characterised by a maximum of heat flow between 10 and 17 h, whereas series A with lower NaOH content of the activator seem to react a little slower. The pure slag pastes (A-S and B-S) are characterised by a maximum of heat flow after about 7 h of reaction at both lower and higher pH of activator solution. The behaviour of the alkali-activated blends differs from that of the pure raw materials metakaolin and slag. The behaviour differs as well for the activator concentrations used in series A and B. The A-25M/75S showed two heat flow maxima, one in the first 2 h of reaction and a second at about 7 h like the pure slag. Then, the heat flow decreases slower than in the reaction of the pure slag. The A-50M/50S mix showed also a little maximum in the first 2 h. Then, the heat flow decreases and remains on a low level at 0.4 mW/g.

At higher activation concentration as used in series B, the heat flow of the blends are characterised by only one significant maximum. The B-25M/75S showed it after about 4 h, the B-50M/50S after about 2.5 h. Then, the heat flow B-50M/50S remains at about 0.7 mW/g. Table 4 includes the detailed data.

Figures 3b and 4b illustrate the heat of reaction versus time of the mix series A and B. Generally, the heat of reaction achieved is higher if a higher activator concentration is used.

The pure metakaolin pastes (A-M and B-M) achieved the highest reaction heat that is still increasing after 74 h of reaction. The slag mixes (A-S and B-S) achieved a lower heat of reaction that seems to come to the end value closely after 74 h.

The A-25M/75S mix achieved middle values between the values of the alkaline-activated pure materials slag and metakaolin. The A-50M/50S mix achieved the lowest heat of reaction.

Using a higher activator concentration increased the heat of reaction of the 50/50-blend (B-50M/50S) in so far as almost the same heat is achieved compared to sample B-25M/75S. These data (heat of reaction after 74 h) are summarised in Tables 4 and 5.

Table 5 Heat of reaction after 74 h, as measured by calorimetry and reaction degree after 28 days as measured by ^{29}Si NMR spectroscopy

Mix	Heat of reaction	Reaction degree by ^{29}Si NMR (mol% Si)[a]		
	$Q_{max\ (74\ h)}$ (J/g)	Metakaolin	Slag	Overall
A-S	29.1	–	0.64	0.64
A-M25/S75	39.0	0.73	0.37	0.50
A-M50/S50	25.0	0.57	0.72	0.62
A-M	49.2	0.42	–	0.42
B-S	43.8	–	0.89[b]	0.89
B-M25/S75	51.2	Not determined		
B-M50/S50	52.4			
B-M	70.9	0.95[c]	–	0.95

[a] Calculated from ^{29}Si NMR results in mol.% Si [13]

[b] By using same procedure as described [13], data published in [14]

[c] By using same procedure as described [13], but data unpublished

Table 4 Series B: measured and calculated data from calorimetric measurement

	t at V_{min} (h)	t at V_{max} (h)	V_{max} (mW/g)	$Q_{(74\ h)}$ (J/g)	Q_{max} (calc.) (J/g)
B-S	1.37	6.52	2.92	43.8	65.3
B-M25/S75	0.77	3.67	2.90	51.2	60.1
B-M50/S50	0.93	2.55	2.42	52.4	80.6
B-M	2.68	12.12	1.74	70.9	83.2

Ultrasonic measurements

Figures 5 and 6 illustrate the velocities of the p-wave over the measurement time for the alkali-activated binders of series A and B. Immediately after mixing, the pastes have a significant damping effect on the ultrasonic waves. Particularly, the metakaolin pastes showed a strong attenuation to such an extent that transmission was completely prevented initially. The ultrasonic pulse velocities that can be measured initially are smaller than the velocities in each individual component air, fluid and solid. These low initial velocities can be attributed to the fact that the air inclusions contained in the system (suspension state) have a substantial influence on the wave propagation [25]. During the further course of structural development, the ultrasonic pulse velocity (see Figs. 5, 6) and signal amplitude increase continuously.

Generally, the pure slag samples (A-S, B-S) achieved the highest p-wave velocity at about 3,000 m/s (A) and 3,700 m/s (B) compared to the pure metakaolin samples that showed a p-wave velocity of about 1,500 m/s (A) and 1,750 m/s (B), respectively, after 74 h. The alkali-activated

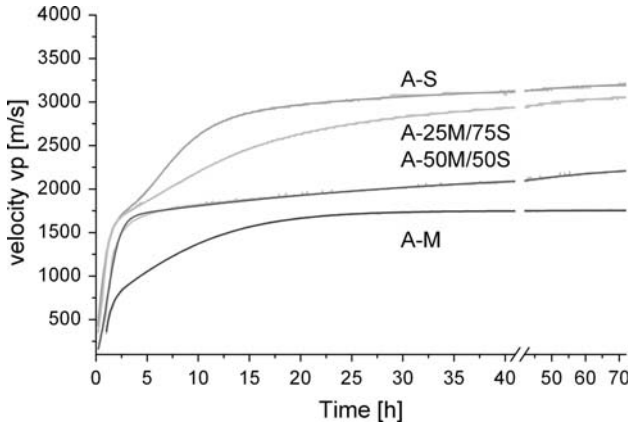

Fig. 5 Results of ultrasonic measurements at low NaOH concentration—series A

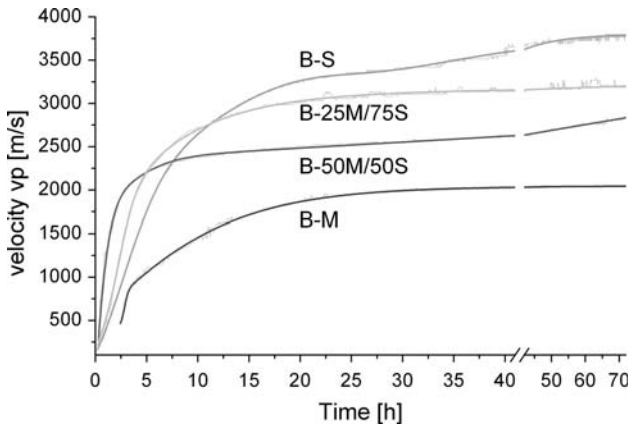

Fig. 6 Results of ultrasonic measurements at high NaOH concentration—series B

blends are in between these values. This correlates to the a higher fluid content of the metakaolin pastes compared to the slag pastes due to a very different water demand and different solid density. All, density ρ and Young's modulus E as well as Poisson's ratio ν have an influence on the p-wave velocity (compare Eq. 1). Additionally, a higher pore volume is expected for the metakaolin pastes than for the slag pastes. This may cause the later onset of initial p-wave transmission at metakaolin pastes.

The curve shape of series A pastes are characterised by a quick and strong linear increase of v_p up to about a half of the end velocity ($\sim$0.4 to $\sim$0.6). This increase occurs in the first 2 h of reaction. The slag containing mixes seem to react similarly attaining a value of about 1,250 m/s within this first increase. Then, the curves separate following a different curve shape. The ultrasonic velocity measured through A-S and A-25M/75S seem to be almost identical in the beginning that is rather interesting because the blend contains a higher water amount. Possibly more reaction product was built in the first 2 h in the A-25M/75S compared to the A-S paste. Then, the pastes show a second strong increase of ultrasonic velocity, but the slope of sample A-S is bigger than the slope of mix A-25M/75S. The ultrasonic velocity measured through blend A-50M/50S increases slightly slower up to about 1,250 m/s, but only a little increase can be measured afterwards. The reaction seems to continue on a very low level that is consistent to the calorimetric data illustrated in Fig. 3. The metakaolin paste A-M shows a different behaviour. The first strong increase with almost linear dependence of the ultrasonic velocity on time passes into a well-formed curvature that seems to reach a constant level at about 1,500 m/s after 40 h of reaction.

The curve shape of the metakaolin sample B-M is similar to the sample A-M with lower activator concentration (Fig. 6). The slag containing samples show a different behaviour at higher concentrations. The reaction seems to be more continuously. Clearly, the blends B-25M/75S and B-50M/50S react much faster than the single activated materials. The mix B-50M/50S shows the highest acceleration. The curves of mix B-M and B-25M/75S seem to reach an end value after 40 h but the velocity of the mixes B-S and B-50M/50S is still increasing.

Discussion

The alkali-activation of ggbf slag, metakaolin and blends of both using NaOH is an exothermic reaction process expressed by two peaks in the heat flow curves, one initial sharp peak—addressed to the wetting of the solid surface together with the dissolution—and a broader second peak—addressed to the heat evolution of the condensation

process. Fernandez-Jiminez [17] concluded for alkaline-activated slag that the reaction kinetic of the condensation step is dominated by the nucleation up to a reaction degree $\alpha \sim 0.1$; whereas

$$\alpha = Q'/Q_{max} \tag{3}$$

and Q_{max} was taken at a heat flow equal or smaller than 0.3 W/g. Therein, a relative heat ("released heat at time t" to "maximum attainable reaction heat") is used as expression for the reaction degree α. Then, the reaction mechanism was characterised by phase boundary interactions. Fernandez-Jiminez [17] concluded as well that the reaction mechanism changes to a diffusion driven process at a hydration degrees α near 0.3 independently on the kind of activator used in their study.

The meaning of value Q_{max} is that of the attainable heat under the existing reaction conditions. Q_{max} will vary if different activators and activator concentrations are used [24]. Therefore, α is the relative heat obtained after a certain time. The comparison of calorimetric and ultrasonic p-wave data of cement concrete or mortar was discussed by Robeyst et al. [26]. Again, the relation $\alpha = Q'/Q_{max}$ was used as comparison base. Therein, Q_{max} was taken after 7 days of calorimetric measurement [27]. The comparison between α and the p-wave velocity illustrated a characteristic bend at α-values around 0.1 that seem to be closely to the time of initial setting measured by penetration test [26, 27].

The difficulties in obtaining Q_{max} are related to:

- not measured heat in the beginning of reaction. That occurs by external mixing and quickly reacting systems [28];
- different methods of obtaining the end value.

Therefore, the values of different studies obtained by different measurement set-ups and calculation methods cannot be compared directly to each other. Nonetheless, an approximate comparison might be possible.

In this work, the values Q_{max} used (as documented in Table 4) were determined by non-linear curve fit. Equation 4 was used for the fitting:

$$y = y_0 + A_1 \cdot \left(1 - e^{-t/b_1}\right) + A_2 \cdot \left(1 - e^{-t/b_2}\right) \tag{4}$$

with y as dependent value Q' from the measurement time t. Therein, the sum of the parameter y_0, A_1 and A_2 gives Q_{max} at infinite time. It should be mentioned that the fitting was primary done with the aim of receiving the maximum attainable reaction heat Q_{max}, rather than determining correct kinetic parameters of the reaction. Finally, it is not clear if the reaction heat will follow these curve progressions in reality, but the usage of a curve fitting rather than a subjective fixed time or heat flow value seems to be more substantial.

Figure 7 illustrates the comparison of the p-wave velocity and the heat flow versus $\alpha = Q'/Q_{max}$ for series B. The heat flow in Fig. 7 is shown from beginning of the

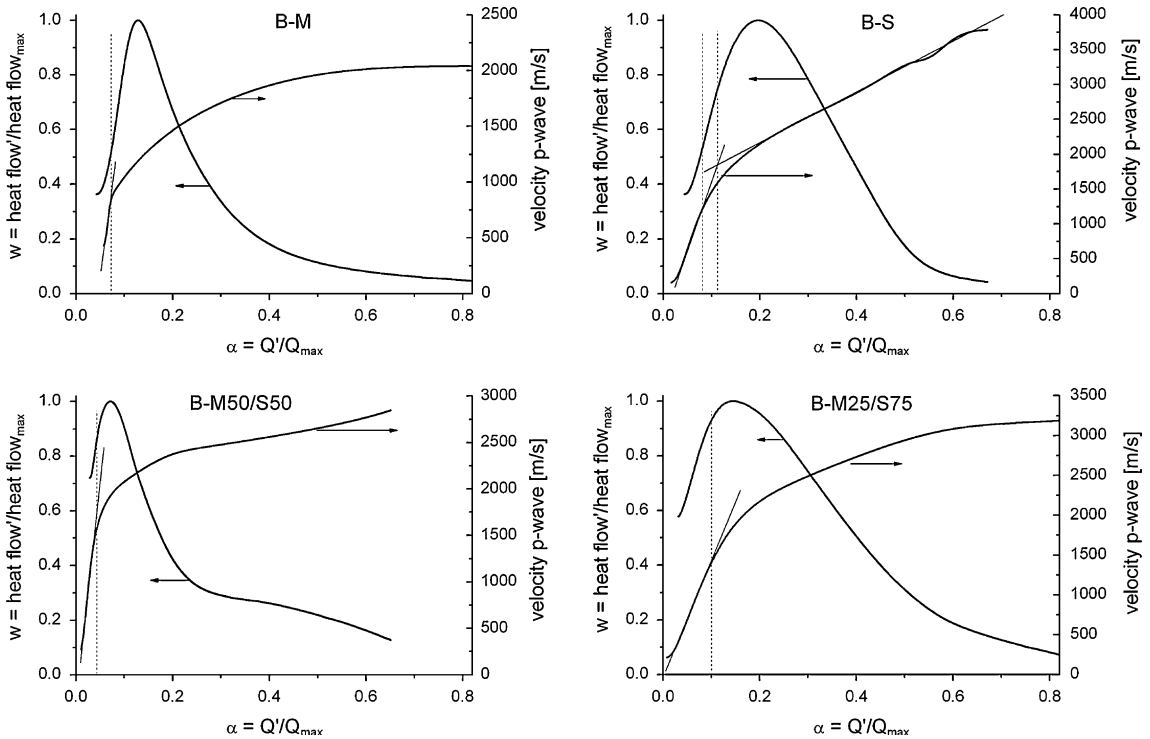

Fig. 7 Series B—reduced heat flow w and p-wave velocity v_p in dependence on the relative heat Q'/Q_{max} released

condensation peak (t at V_{min}) and inserted as normalised heat flow w:

$$w = V'/V_{max} \quad (5)$$

with V'—heat flow at certain time t' and V_{max}—heat flow maximum of the condensation curve; the values are documented in Table 4.

Figure 7 illustrates the different characters of the alkaline activation of ggbf slag and metakaolin both in the heat flow curve and in the p-wave velocity data. The reaction of metakaolin is characterised by quick increasing of the p-wave velocity almost linear to α and a significant bend at $\alpha \sim 0.08$ and $v_p \sim 900$ m/s. The velocity data passes into a curvature and lately in a straight line at $v_p \sim 2{,}050$ m/s. In contrast to the ultrasonic data, the heat evolution is still increasing (compare Fig. 4).

The behaviour of alkaline-activated slag is different to the metakaolin. The ultrasonic data are characterised as well by a strong increasing of the velocity up to an $\alpha \sim 0.08$ and $v_p \sim 1{,}300$ m/s. Then, the increasing follows still a linear dependence on α with a lesser slope. The intersection of both lines are to be found at $\alpha \sim 0.11$.

Herb [27] discussed this point as the border between setting and hardening indicating the final setting. Reflecting that is has to be mentioned that the distinction between setting and hardening is only a subjective one and indicates the realisation of a defined limit of Young's modulus. The steady increase of the p-wave indicates the steady ongoing of the structure forming reaction (condensation). The intersection points to the slope changing of the velocity increase that possibly indicates a changeover of two reaction mechanism.

The onset of slag containing mixtures at relatively low velocities and their linear increase in the beginning of the reaction indicates an early start of the structure formation. Unfortunately that cannot be seen for the metakaolin paste due to a higher damping of the ultrasonic waves. That means the nucleation starts at very early reaction times. This information cannot be seen in isothermal calorimetry due to the overlaying of the heat evolution of dissolution and condensation step.

The blended systems seem to show an overlapping of two (condensation) reactions, clearly seen in the calorimetric data of B-50M/50S mix (see Fig. 7) and of A-25M/75S mix (see Fig. 3). The calorimetric data of B-50M/50S mix in Fig. 7 illustrate the appearance of a second hidden peak in the heat flow curve with its maximum at $\alpha \sim 0.4$. Possibly either the metakaolin or the slag is still reacting. The first heat flow maximum appeared after 2.6 h (see Table 4). The heat flow maximum of the B-25M/75S mix appeared after 3.7 h. That is significant earlier than the heat flow maximum of the single activated materials slag and metakaolin with 6.2 and 12.1 h, respectively. The ultrasonic measurement results underlay this statement of a parallel reaction of the metakaolin and the slag as illustrated in Fig. 7. The quick and strong increase of the p-wave velocity is obvious, but is not followed by a well-formed curvature or by a line. Additionally, the structure forming appeared as well to earlier time than the single activated materials as illustrated in Fig. 6.

The reason of the acceleration of the condensation reaction is the release of aluminium from metakaolin and its incorporation into the calcium silicate hydrate phases. The same acceleration effect is used by the addition of sodium aluminates as setting accelerator for shotcrete or as aluminium hydroxides to improve the early strength of slag cements [29].

Conclusions

Blends of metakaolin and ggbf slag were alkali-activated using a low and a higher concentrated NaOH solution as alkaline activator. The reaction progress was followed by conduction calorimetry as well as by ultrasonic transmission measurements.

A clear interaction of the both solid raw materials could be seen in the calorimetric measurements. The condensation reaction is accelerated by the blending of slag and metakaolin. This is noticeable at both concentration levels, but the influence is much apparent at higher concentrations. This can be explained by a higher amount of dissolution of both slag and metakaolin, but it is more significant on metakaolin dissolution.

The high aluminium content of the metakaolin now available in pore solution accelerates the condensation of the calcium silicate hydrates by incorporation of the aluminium tetrahedra.

The acceleration effect is seen not only in calorimetry, but also in the ultrasonic measurements. The acceleration effect is more noticeable at higher activator concentrations. The ultrasonic measurement illustrates very well the early phase formation that started closely after mixing. A strong increase of the p-wave velocity is noticeable in the very beginning of the condensation that was identified in all mixes. About 50% of the velocity is attained in the beginning of the reaction when only about 10% of the reaction heat is emitted. This rapid increase of the ultrasonic velocity is followed by a slower increase with different curve shapes of the metakaolin and slag mixes. The dramatic change in p-wave velocity indicates the changing from a paste to a solid. From the time the (slag or metakaolin) grains getting connected, the increase of p-wave velocity is slowed down. The development of ultrasonic velocity in the solid material in which the reaction is still ongoing seems to be different for the slag and the

metakaolin probably due to the different reaction product formed. That behaviour of alkaline-activated slag and metakaolin will be the object of further investigation.

References

1. Davidovits J (1976) In: IUPAC international symposium on macromolecules. Topic III, New polymers of high stability, Stockholm
2. Davidovits J (1999) In: Davidovits J (ed) Proceedings of the second international conference geopolymere '99, St. Quentin, France, p 9
3. Kühl H (1908) US Patent 900939
4. Purdon AO (1940) J Soc Chem Ind 59(9):191
5. Schilling PJ, Butler LG, Roy A, Eaton HC (1994) J Am Ceram Soc 77(9):2363
6. Wang S-D, Scrivener KL (2003) Cem Concr Res 33:769
7. Richardson IG, Brough AR, Brydson R, Groves GW, Dobson CM (1993) J Am Ceram Soc 76(9):2285
8. Scrivener KL, Wang S-D (1995) Cem Concr Res 25(3):561
9. Granizo ML, Alonso S, Blanco-Varela MT, Palomo A (2002) J Am Ceram Soc 85(1):225
10. Palomo A, Blanco-Varela T, Alonso S, Granizo L (2003) In: Proceedings of the 11th congress on the chemistry of cement (ICCC), Durban, South Africa, p 425
11. Yip CK, van Deventer JSJ (2003) J Mater Sci 38:3851. doi: 10.1023/A:1025904905176
12. Yip CK, Lukey GC, van Deventer JSJ (2005) Cem Concr Res 35:1688
13. Buchwald A, Hilbig H, Kaps C (2007) J Mater Sci 42(9):3024. doi:10.1007/s10853-006-0525-6
14. Hilbig H, Buchwald A (2006) J Mater Sci 41(19):6488. doi: 10.1007/s10853-006-0755-7
15. Alonso S, Palomo A (2001) Cem Concr Res 31(1):25
16. Granizo ML, Blanco MT (1998) J Therm Anal 52:957
17. Fernandez-Jimenez A, Puertas F, Artega A (1998) J Therm Anal 52:945
18. Gruskovnjak A, Lothenbach B, Holzer L, Figi R, Winnefeld F (2006) Adv Cem Res 18(3):119
19. Tatarin R, Erfurt W, Stark J (2004) ZKG Int 57(8):69
20. Grosse CU, Reinhardt H-W, Krüger M, Beutel R (2006) In: Reinhardt H-W (ed) Proceedings of the advanced testing of fresh cementitious materials, Stuttgart, p 83
21. Lawson JL (2008) Diploma thesis for the degree of Master of Science in Mechanical Engineering, Rochester Institute of Technology, Rochester, NY. https://ritdml.rit.edu/dspace/bitstream/1850/7356/1/JLawsonThesis09-2008.pdf. Accessed 27 July 2009
22. Lawson J, Varela B, Panandiker RSP, Helguera M (2008) In: Lin H-T, Koumoto K, Kriven WM (eds) Developments in strategic materials: ceramic engineering and science proceedings, vol 29, issue 10, p 143. ISBN: 978-0-0470-34500-9
23. Granizo ML, Blanco-Varela MT, Palomo A (2000) J Mater Sci 35:6309. doi:10.1023/A:1026790924882
24. Shi C, Krivenko P, Roy D (2006) Alkali-activated cements and concretes. Taylor and Francis, London, p 376. ISBN: 0-4157-0004-3
25. Sayers CM, Dahlin A (1993) Adv Cem Based Mater 1:12
26. Robeyst N, Gruyaert E, Grosse CU, Belie ND (2008) Cem Concr Res 38:1169
27. Herb A (2003) Indirekte Beobachtungen des Erstarrens und Erhärtens von Zementleim, Mörtel und Beton mittels Schallwellenausbreitung. Universität Stuttgart, Stuttgart
28. Fernandez-Jimenez A, Puertas F (1997) Cem Concr Res 27(3):359
29. Wassing W, Tigges VE (2008) Cem Int 6(5):62